SCIENTIFIC REPORTS

OPEN

SUBJECT AREAS:
MAGNETIC PROPERTIES AND MATERIALS
INFORMATION STORAGE
NANOPARTICLES
SCANNING PROBE MICROSCOPY

Received
12 September 2012

Accepted
9 April 2013

Published
23 April 2013

Correspondence and requests for materials should be addressed to D.R.-M. (druiz@cin2.es)

Robust spin crossover platforms with synchronized spin switch and polymer phase transition

F. Novio, E. Evangelio, N. Vazquez-Mera, P. González-Monje, E. Bellido, S. Mendes, N. Kehagias & D. Ruiz-Molina

Centro de Investigación en Nanociencia y Nanotecnología (ICN-CSIC), Esfera UAB, 08193 Cerdanyola del Vallès, Spain.

The idea of developing magnetic molecular materials into real functional electronic devices with low-cost and scalable techniques appeared with the emergence of the field several years ago. Today, even though great advances have been done with this aim, the promise of a functional device working at the micro-/nanoscale and at room temperature has unfortunately not completely materialized yet, as their use still strongly depends on the fabrication methodology of a robust device that can be handled and integrated without compromising their functionality. Here we propose the use of polymeric matrices as a platform for the development of such robust switchable structures exhibiting reproducible results independently of the dimension -from macro to micro-/nanoscale- and morphology -from thin-films to nanoparticles and nanoimprinted motives- while allowing to induce an irreversible hysteresis, reminiscent of a non-volatile memory, by synchronization with the polymer phase transition.

Coordination complexes involving a reversible switching process between two electronic isomers with different spin ground states in response to external stimuli are of growing interest in the area of functional materials[1]. The different magnetic properties exhibited by both isomers, which are also accompanied by variations of the optical properties[2,3], can be easily tuned under the influence of various external parameters such as temperature, pressure or light irradiation[4,5] opening up a broad range of possible applications in sensor, display and information storage[6]. For this to be achieved, controlled fabrication of robust micro-/nanostructures with high potential device integration is required[7]. Numerous reports on the preparation of micro-/nanostructured materials based on switchable coordination complexes, such as spin crossover (SCO)[8] or valence tautomerism (VT)[9], in less extent, have been reported over the last years. Particles with different size/properties correlation[10,11] thermal hysteresis loops[12] and the possibility to be scaled down to a few nanometers with a narrow size distribution have been reported[13]. A switchable molecular device obtained by contacting an individual nanoparticle based on spin-crossover molecules between nanometer-spaced electrodes has also been reported[14]. (Multi)layer thin-films[15,16], that can be (nano)structured by different lithographic techniques[17,18], a combination of sequential assembly and electron beam lithography techniques[19] or a memristance systems[20] have also been reported. Even though large advances have been made in this sense, the switching behaviour still differs in an unpredicted manner from that observed for bulk samples, except in some cases[21,22]. This fact, together with the limited control existing for their positioning and integration by cost-effective and easily scalable manufacturing processes, poor surface stabilities or their critical dependence on the local molecular environment (e.g. packing, solvent molecules, anions, etc.)[23] still make necessary the development of proper methodologies for the fabrication of robust and feasible micro-/nanostructures with potential integration into functional devices[24].

On a relevant step forward, here we show that it is possible to convert the spin crossover observed in a polymeric matrix[25] in a viable alternative for the fabrication of such robust micro-/nanoplatforms, with a proper stability and robustness and the corresponding technological relevance that it involves. Moreover, it is also possible to control the switchable behavior in a predicted manner[26], by being synchronized with the polymer nature and its glass transition temperature.

Results

Ambient fabrication and optimization of polymeric composites. Complex [Co^{III}(Cat-N-SQ)(Cat-N-BQ)] (**1**,*ls*-Co(III)) exhibiting a VT interconversion was the molecule of choice for these studies[27]. The most stable

1, *ls* form at low temperature interconverts to the high spin form $[Co^{II}(Cat\text{-}N\text{-}BQ)_2]$ (**1**, *hs*-Co(II)) upon an increase of the temperature in a reversible manner, as schematically depicted in Figure 1.

The reversible interconversion between the different electronic isomers can be followed by variable-temperature UV-Vis spectra as shown in Figure 2a. In spite this phenomenon arises from an exclusively intramolecular electron transfer (IET) process involving the metal ion and the redox active ligand, related with that observed for Prussian blue analogues[28,29], electron-phonon coupling and the elastic properties of the matrix strongly influence its interconversion; it can be shifted to much higher temperatures, from abrupt to smooth, or even disappears depending whether it is in solution or in solid state, crystalline or amorphous[30]. Therefore, handling of **1** on solid surfaces or as particles, while maintaining their characteristic VT behaviour in a predictable manner, represents a real challenge to demonstrate the validity of our polymeric approach.

Optimization of the polymeric composite targeting for a successful stable final processed material was tested at three different concentrations (2% wt., 4% wt. and 8% wt.) in poly(methyl methacrylate) (PMMA), a well-known polymer of relevant technological interest that can be structured both on surfaces or as particles. In a typical experiment, a 15% wt. of the polymer is dissolved in dichloromethane whereupon complex **1** is added. The resulting mixtures are deposited on a glass slide by drop casting methodology, resulting in thin-films that oscillate between 5 and 20 microns width that can be handled and transferred onto different substrates. Afterwards the existence of VT was studied by variable-temperature UV-Vis spectroscopy in the 163–373 K temperature range. Best results were obtained for the 2% wt. thin-film that exhibit an interconversion very similar to that found for a related toluene solution (see Figure 2c) centred at room temperature, for many consecutive heating/cooling processes. An increase of the concentration even only up to 4% wt. modifies the equilibrium by favouring the percentage of the **1**,*hs-Co(II)* isomer present over the same temperature range, being more evident at 8% wt., where only such isomer is detected by UV-vis spectroscopy (see Supplementary Material). This fact has been attributed to the crystallization of **1** at concentrations beyond 2% wt., as confirmed by polarized optical microscopy and X-Ray diffraction (XRD) techniques. Optical microscopy images revealed a good dispersion of **1** within the matrix at the lowest concentration of 2% wt., with no evidences of phase segregation either crystallization. An increase of the concentration up to 4% wt. already induces the appearance of some crystalline seeds not well defined until the concentration reaches 8% wt. The presence of crystals with dimensions below the optical resolution limit was confirmed by XRD. No pattern beyond that of the background substrate can be observed for the pristine and 2% wt. thin-films whereas more clear and defined peaks are observed at 4% wt. and especially at 8% wt (this was a general tendency found for other polymers of different nature such as poly (vinyl alcohol) (PVA) or poly(bisphenol) A carbonate (PBC), see Supplementary Material). In addition, such XRD patterns are characterized by the presence of a few peaks, much less than expected from the powder diffraction data of an anisotropic polycrystalline sample, fact that has been interestingly attributed to a preferential growth of crystallites within the thin-films (see Supplementary Material).

Far from being an inconvenient, the tendency to form crystals within the polymeric matrix was used to adapt our volatile switchable behaviour (which recovers its initial state after removing the external stimuli without any hysteresis) on a permanent non-volatile memory in a controlled manner. If the 2% wt. thin-film of complex **1** is heated up to 403 K, just above the PMMA T_g, and allowed to rapidly recover room temperature, the thin-film retains its amorphous character and therefore the corresponding reversible switchable behaviour. On the contrary, if room temperature is slowly recovered (1 $K.min^{-1}$ or less), crystallization of **1** takes place within the polymeric matrix as confirmed by optical microscopy (see Supplementary Material). Since crystals of **1** were found to be stabilized on its *hs-Co(II)* form, as previously described, the characteristics of the high-spin isomer are retained in this way upon cooling in an irreversible manner down to room temperature, and after several heating/cooling cycles. This represents a new strategy to synchronize VT and phase transition at will by means of the external polymer, without the need of any demanding additional synthetic route[31]. Once the best experimental conditions for the fabrication of the polymeric matrix were established, the next step was its structuration both as particles and structured surfaces, key steps for the development of devices.

Micro-/nanostructuration in bulk. PMMA particles were first obtained by a solvent evaporation method; the organic solvent containing the polymer and complex **1** with concentrations similar to those used for the thin-films, was emulsified in an aqueous phase inducing a precipitation of the polymer as spherical particles after solvent removal, trapping inside complex **1**. Figure 3a shows the electron micrographs (SEM/TEM) of the resulting particles with an average diameter that can go from a a few micron to hundreds of nanometers. More interestingly, their magnetization temperature dependence ($\chi_M.T$ *vs.* T) in the 250–350 K temperature range under an external applied magnetic field of 1 T confirmed the maintenance

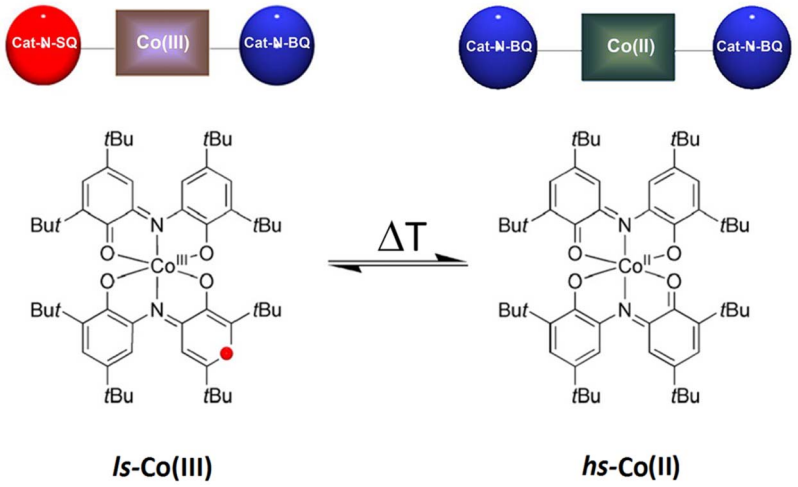

Figure 1 | Valence tautomerism. Electronic isomers involved in the VT equilibrium of complex 1 and schematic representation where the different electronic states of the ligands and metal ion are represented by geometric figures with a colour code.

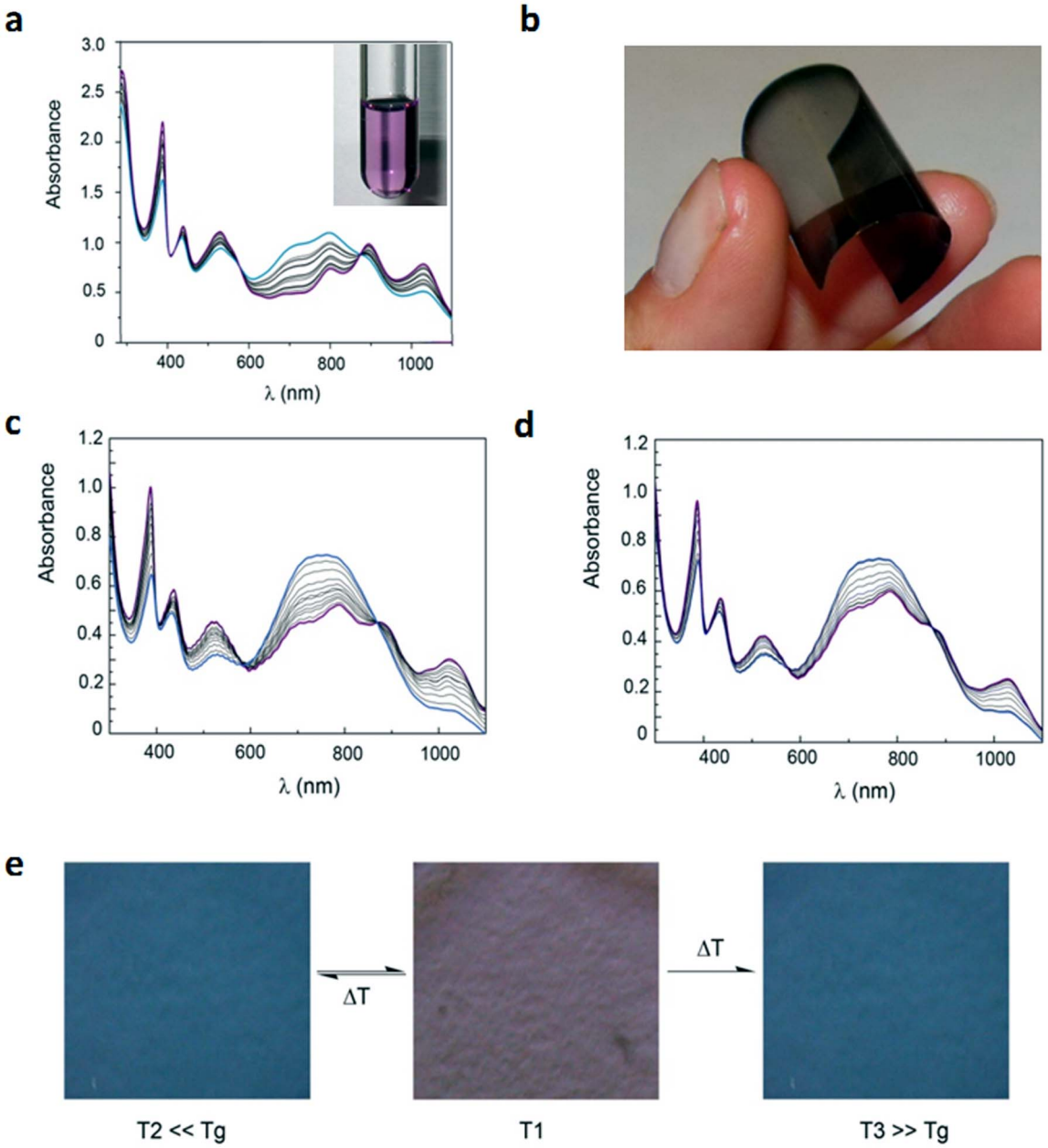

Figure 2 | Variable-temperature dependence. (a) Variable-temperature UV–Vis spectra of a toluene solution of 1 in the 200–350 K temperature range (Inset: image of the solution at room temperature). Bands at 391, 439 and 533 nm characteristic of the 1,ls-Co(III) isomer can be observed in the low-temperature regime (magenta spectrum). As the temperature is increased, the intensity of such bands decreases whereas bands at 721 and 797 nm characteristic of the 1,hs-Co(II) isomer increase in intensity, with two clear isosbestic points at 856 and 590 nm. (b) Image of a flexible PMMA thin-film containing 2% wt. of 1. (c) Variable-temperature UV–Vis spectra of the thin-film shown in (b) upon heating from 163 to 373 K, where a similar variation to that found in solution can be observed. (d) Variable-temperature UV–Vis spectra of the thin-film shown in (b) upon cooling from 373 to 163 K. (e) Photographs of a 2% wt. PMMA thin film of 1 at different temperatures. The magenta-like colour found at room temperature (middle image) changes to cyan in a reversible manner when heated below Tg (left image) and irreversibly if heated above Tg (right image).

of the switchable behaviour. At low temperatures, the observed χ_M.T value is 0.4 emu.K.mol^{-1} in agreement with dominance of the low-spin isomer **1**,*ls*-Co(III) bearing one unpaired electron. This value remains approximately constant up to 300 K, whereupon a gradual increase of the magnetic moment up to a χ_M.T = 0.8 emu.K.mol^{-1} at 350 K, associated with the incomplete interconversion to the **1**,*hs-Co(II)* isomer, is observed. Such temperature-induced reversible interconversion was also followed by a particle colour change by means of an optical microscope (see Figure 3b).

Micro-/nanostructuration on surfaces. Another challenge successfully faced in this work was the structuration of the same composite on surfaces by means of different lithographic techniques. Initially, Dip-Pen nanolithography (DPN) was the technique of choice for this since has evolved as a very promising technique for structuring a wide range of substances on surfaces at the nanometre scale, due to its direct-writing and high resolution capabilities[32]. Initially, several experiments were performed to establish the best experimental conditions for the deposition of pure PMMA polymer on cleaned silicon surfaces by controlling the contact (dwell) time of the PMMA-coated tip with the target surface (1, 2, 3 s) and the substrate temperature. Optimized conditions were found for a substrate temperature of 443 K, well above T_g (395 K) of our PMMA but below the decomposition temperature of **1** (478 K),

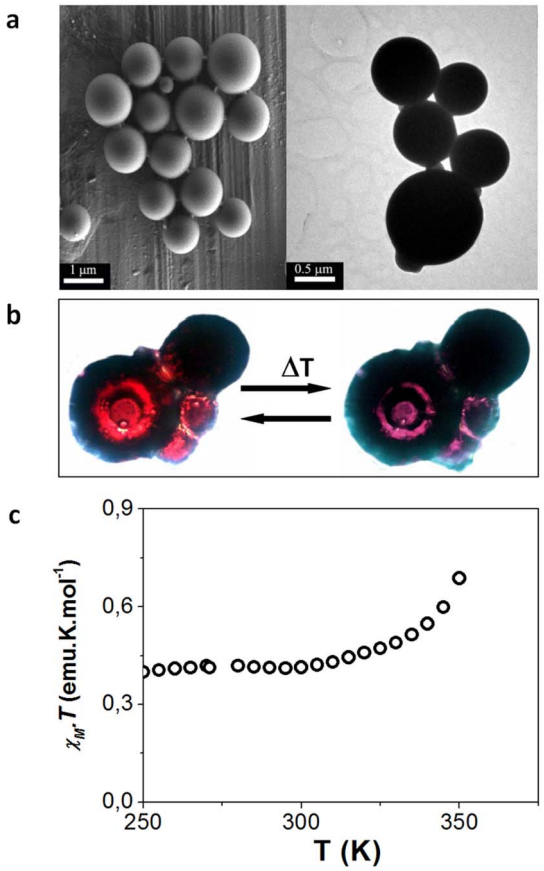

Figure 3 | Variable-temperature and morphological characterization of the PMMA/1 particles. (a) SEM (left) and TEM (right) images of PMMA particles doped with a 2% wt, of complex 1. (b) Variable-temperature dependence of the particles shown in (a) along the 300–373 K temperature range followed by optical means (colours may differ from the photographs shown in Figure 2 due to optical restrictions of the optical microscope camera). (c) Temperature dependence of cM.T in the 250–350 K temperature range under an external applied magnetic field of 1 T of the particles shown in (a). An uncompleted VT can be observed along the 300–350 K temperature range.

and a contact time of 3 s. Under these conditions, well defined arrays of dots with 2.3 ± 0.1 μm and 12 ± 1 nm of diameter and height, respectively, are obtained scanning the tip over the surface (see Supplementary Material). A detailed study of the generated structures by Atomic Force Microscopy (AFM) reveals that each one of the dots exhibits a fibre-like structure independently of the cooling ramp applied after the deposition process (from 0.2 to 10.0 K/min). The same experimental conditions were used afterwards for the deposition of the PMMA bearing now a 2% wt. of complex **1**, resulting in the formation of well defined and reproducible arrays with average dot diameters of 1.5 ± 0.1 μm and 111 ± 5 nm height (see Figure 4). Moreover the dots reproduce the fibre-like structures previously found indicating no effect of complex **1** over the final dot morphology.

Nanostructured motives on cleaned silicon surfaces were alternatively fabricated in an easy and reproducible manner by Nanoimprint Lithography (NIL), which is easily scalable to macroscopic areas by related techniques such as roll-to-roll. In a typical experiment, a solution of complex **1** and PMMA with a similar ratio to that used for the fabrication of the thin-films, is spin-coated on a silicon surface heated above the PMMA T_g and the stamp brought into contact under pressure. Afterwards, the system is cooled down as fast as possible to avoid crystallization processes while the mold is separated from the sample resulting in a negative replica of the stamp on the film. A reactive ion etching, was finally used to transfer the pattern in the resist to the underneath substrate (see Figure 5a). Optical images show patterned motives with different shapes, ranging from squares to circles or lines, and dimensions down to almost 1 μm. Detailed SEM images of representative polymeric motives with triangular and donuts-like structures are also shown in Figure 5c. More interestingly, variable-temperature diffuse reflectance UV-Vis spectra (193, 298 and 353 K) of a silicon oxide piece covered with a NIL nanostrucutred films showed that the same composite once structured on a surface retains the switchable behaviour. As showed in Figure 5d, bands at 391, 439 and 533 nm characteristic of the **1**,*ls*-Co(III) isomer can be observed in the low-temperature regime that decrease in intensity as the temperature is increased, whereas bands at 721 and 797 nm characteristic of the **1**,*hs*-Co(II) isomer increase in intensity, with two clear isosbestic points at 856 and 590 nm. This behaviour is reminiscent for the VT of complex **1** found in solution and the polymeric thin-films.

Discussion

We have shown that the fabrication of optimized polymeric composites by controlling both the nature of the polymer and the concentration of the spin crossover molecular material allowed us to develop a new break-through experimental approach for the fabrication of a broad range of functional switchable micro-/nanostructures, from thin-films to particles or nanostructured surfaces. On increasing the temperature below the glass transition of the polymer, while working at concentrations low enough to avoid crystallization, such structures exhibit magnetic and optical responses that can be switched back in a reversible manner after cooling, without any remarkable fatigue. If heated above, a slow cool down induces the formation of crystals of the complex within the structure, which is used to block one of the states in a reminiscent manner of a non-volatile memory. Our results open a pathway towards the design of operable molecular electronic and optical devices with controlled switchable functionalities and high integration capacities.

Methods

Complex **1** was synthesized as previously reported[19]. Commercially available reagents were used as received. All reagents were acquired at Sigma-Aldrich with 99% purity. The characteristics of the commercial polymers used were as follows: PBC (Mw = 64000 g/mol, PDI = 1.45) and PMMA (Mw = 350000, PDI = 1.10).

Thin-film fabrication. In a first step the polymer is dissolved in 10 mL dichloromethane (DCM) with a concentration of 15% wt. (0,150 g) and afterwards complex **1** is added on the resulting mixture with selected concentrations (2%, 4% and 8% wt.). After vigorous stirring the mixture is left to repose for at least 10 minutes and subsequently casted onto a glass substrate. During the drop casting the glass plate was placed in a closed chamber (with anhydrous sodium sulphate) in order to control the initial evaporation of the solvent from the prepared film and avoiding the water molecules. After this first evaporation step of the solvent, the films where characterized without being depleted from the substrate. For the characterization samples with relative large plane surfaces, homogeneous and without pinholes were required.

Particle fabrication. *Microparticles*. In a typical procedure, an homogenous dichloromethane solution (15.5 g) of PMMA (0.56 g) and VT-complex (11 mg) was added drop by drop to a beaker containing 103.5 g of SDS/PVP aqueous solution (4.5 g/9 g respectively) while emulsified using an IKA ULTRA-TURRAX (T25 digital) disperser at 10.000 rpm. This emulsion was then poured into a 250 mL round bottomed flask and dichloromethane was subsequently evaporated by heating at 323 K and stirring with a magnetic stirrer at 500 rpm over night in the uncovered flask. The resulting particles were collected by filtration and washed thoroughly with water to remove SDS/PVP excess. Filters with different pore sizes were used to enhance monodispersity.

Nanoparticles. In a typical procedure, 4 mL of a dichloromethane solution containing PMMA (100 mg) and VT-complex (2 mg) was added into 10 mL of a 1% PVA aqueous solution. The mixture was emulsified using an IKA ULTRA-TURRAX (T25 digital) disperser at 24.000 rpm in an ice bath. Dichloromethane was subsequently removed from the emulsion by evaporation at room temperature under magnetic stirring (300 rpm, 1.5 h). The resulting particles were washed and collected by redispersion in distilled water and centrifugation (15.000 rpm for 5 min, ×3).

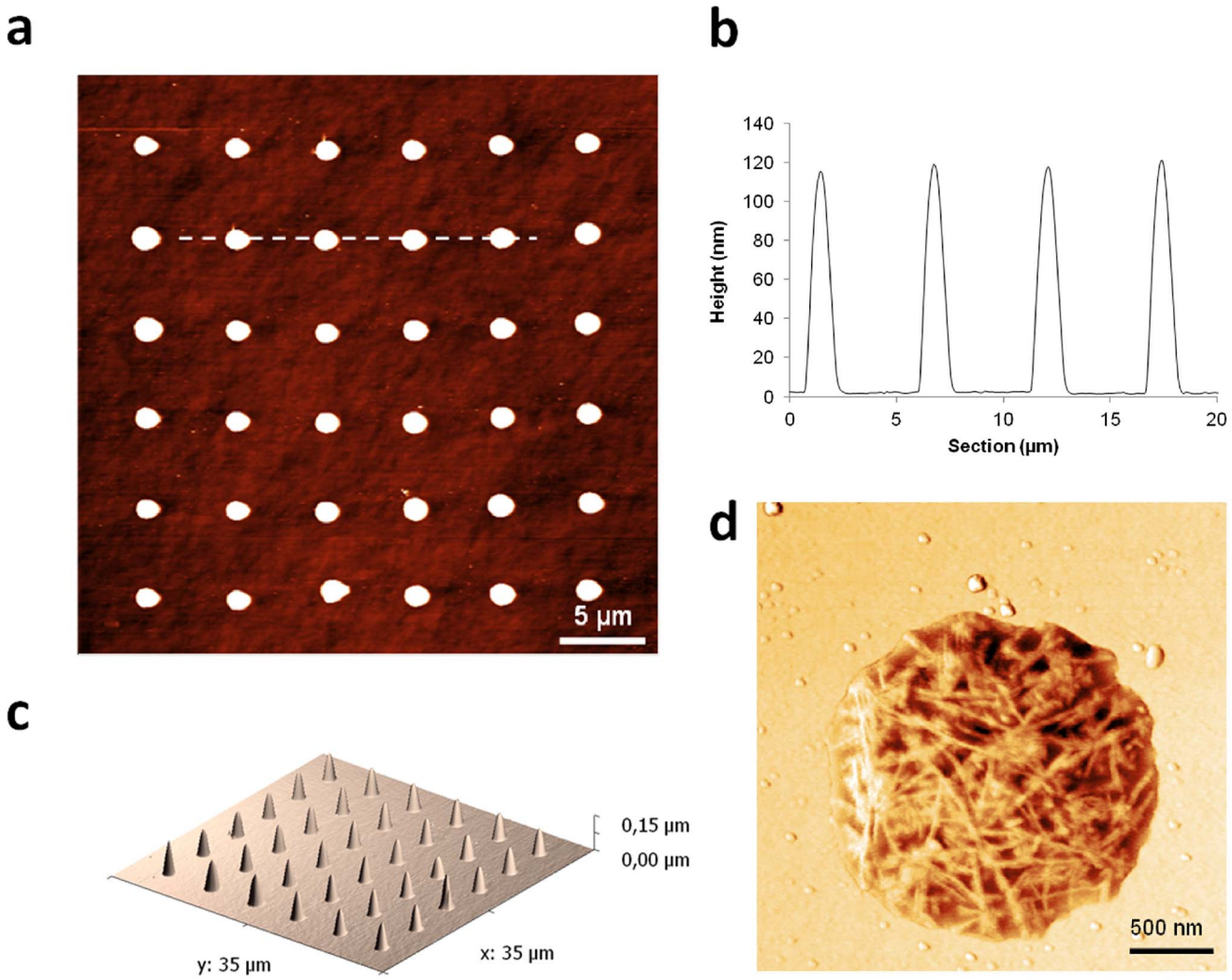

Figure 4 | DPN patterned arrays. (a) AFM topography image of an array made of repeated dots 1.5 ± 0.1 μm in diameter spaced by a distance of 4 μm. (b) Height profile associated to the rows shown in panel (a). (c) 3-D AFM topography image of the array shown in (a). (d) Amplified AFM phase image of one of the dots shown in panel (a).

Dip-pen nanolithography. Solid PMMA was dissolved in 1,2-dichlorobenzene (*o*-DCB) obtaining a 15% wt. solution. The diluted 1:10 polymer solution was used as ink in DPN experiments. DPN experiments were performed with a commercial dip-pen writer: NSCRIPTOR™ DPN System (Nanoink Inc.). All experiments were carried out at ambient conditions (~35% relative humidity and room temperature) although increasing the substrate temperature Ts up to 420–450 K. An *o*-DCB solution of PMMA (15% wt.), where the polymer acts as a carrier for the valence tautomeric complex **1** that was added (2% wt. of the total), is the second ink used. Silicon substrates were cleaned carefully by immersion in piranha solution (H_2SO_4/30% H_2O_2 = 3/1 (v/v)) at room temperature for 30 minutes. The silicon substrates were washed several times by rinsing with deionized water and methanol and dried with N_2 flow. DPN-probes were used without any pretreatment (provided by Nanoink Inc.). Tips used were M-Type Pen consisting of 12 silicon nitride parallel cantilevers with sharpened pyramidal tips with a low spring constant (0.5 N/m). The temperature of the substrate was set from ambient temperature to 523 K by using a high temperature stage (Agilent 5500 AFM/SPM microscope). The setpoint temperature (Ts) was fixed in the temperature control stage, being the temperature on the silicon substrates ~20% lower than Ts. In order to coat the M-Type Pen with the PMMA solution the tips were brought into contact in a microfluidic ink delivery chip-based system named inkwell (Nanoink Inc.). The coating was performed by dipping the tips in the ink-filled reservoirs after heating and stabilizing the PMMA solution at 420 K because of the viscosity of the solution. Once the tips were coated, Ts was raised to 453 K and they were brought into contact with the substrate to remove the polymer excess and be able to create defined nanostructures. Then, polymer nanoarrays were generated on the silicon surfaces by traversing the tip over the surface in the form of the desired pattern. Dot arrays were prepared at different tip-substrate contact times (1, 2 and 3 s) and Ts (423, 433, 443 and 453 K). Periods of 2–3 min of the tip contacting the substrate were performed before each lithography to reach thermal equilibrium on the M-Type pen array. The cooling step of the nanoarrays was performed by turning off the high temperature stage and letting the substrate reach the ambient temperature.

Experiments were performed proceeding exactly in the same way although decreasing the Ts after the lithography with a ramp of 0.2 K/min. The deposition of the ink solution containing the complex 1 embedded in the PMMA matrix was carried out at a Ts of 423 K, avoiding increasing the temperature above the Td where the complex loses the valence tautomeric behaviour, and 3 s of tip-substrate contact time in order to have a high concentration of complex 1 inside the generated structures.

Nanoimprint lithography. Procedure: stamp and substrate are brought into contact. The temperature is set to a value of 343–353 K above the glass transition temperature of the polymer film, while a pressure is applied to facilitate the polymer flow inside the stamps cavities. The assembly is kept to this temperature and pressure for several minutes. The stamp and substrate are separated at 283–288 K lower than the polymer glass transition temperature. The remaining residual layer could be either etched or not, depending on the targeted application.

UV-Vis diffuse reflectance measurements. UV-Vis spectra of the nanostructured tin film were obtained at different temperatures using a Jasco V550 UV/Vis spectrophotometer (wavelength accuracy <1 nm) with an integrating sphere attachment installed. The spectra were recorded in the 300–1100 nm range using PMMA as reference. The instrument was equipped with a thermostatic cell holder that can operate between 180 and 370 K. Spectra were collected after the sample had been allowed to thermally equilibrate at each temperature for 15 min.

Physical measurements. *Electronic absorption measurements.* The spectra were recorded on a Perkin Elmer Lambda 35 spectrophotometer. The instrument was equipped with a thermostatic cell holder that can operate between 180 and 370 K.

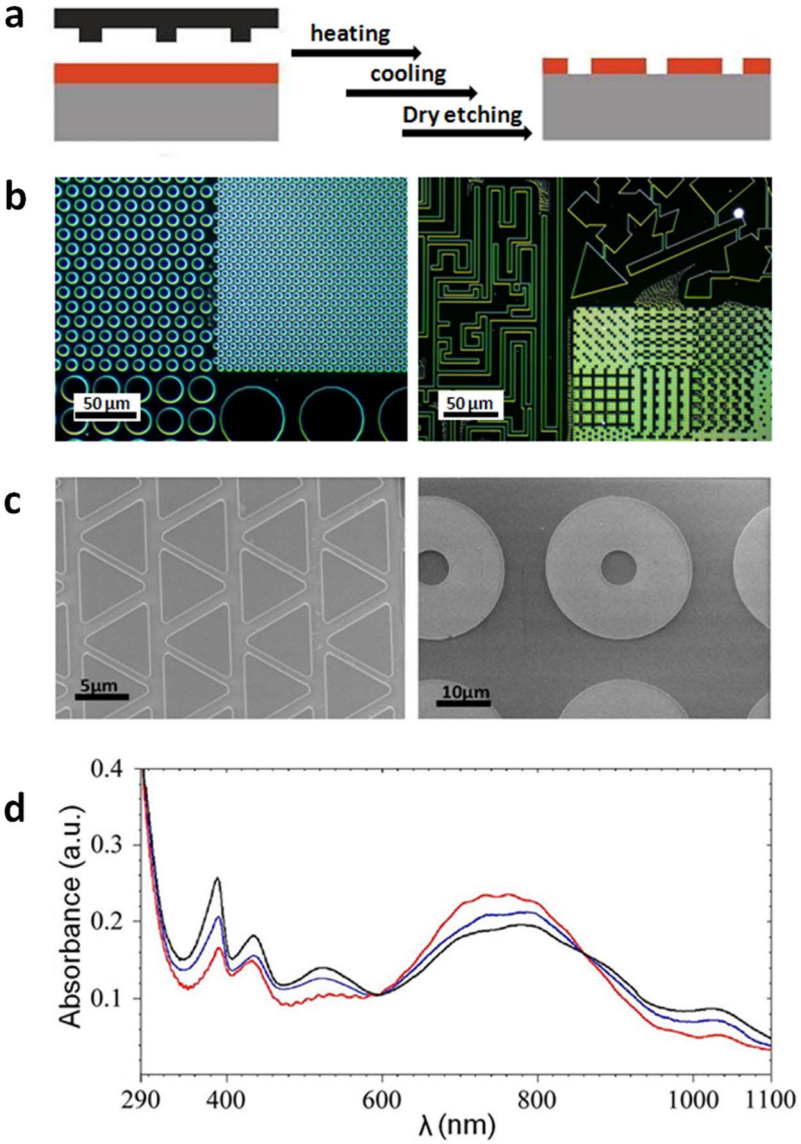

Figure 5 | Nanoimprinting lithograpy and variable-temperature reflectance diffuse studies of surface structured motives. (a) Schematic representation of the NIL process used for the fabrication of the structures over a thin-film obtained by spin coating. (b) Optical microscopy images of the different motifs that can be achieved with the stamp used in these experiments. (c) SEM images of selected triangular and donuts-like motifs. (d) Variable temperature electronic spectra of a nanostructured PMMA thin-film containing 2% wt. of 1. Colour code: 193 K (black), 298 K (blue) and 353 K (red).

Temperature stability was better than ±5 K. The spectra were recorded in the 300–1100 nm range using PMMA as reference. Spectra were collected after the sample had been allowed to thermally equilibrate at each temperature for 15 min. In some specific experiments, Tc, the temperature at which the isomer ratio is 1 : 1, was deduced from the temperature at which the peaks of the low-spin and the high-spin exhibit similar intensities. The N2 was the carrier gas used in the cooling and heating programmes.

X-ray diffraction. The data have been recorded on an INEL Diffractometer (Debye-Scherrer geometry and CPS120 curved detector) which collects 393 K of the diffraction circle using the Kα radiation of copper. The sample was introduced in the diffractometer in capillars of 0.3 mm.

Optical microscopy. Zeiss Observer was used to investigate the structure of the complex in the different polymeric matrixes. This method is sensitive and the samples for the optical microscopy measurement is placed in the microscope plate and observed with different objectives (5, 10, 20, 50 and 100x). Optical microscopy with polarized light was carried out with an Optical Microscope Leica DMRB and a Stereoscopical LUPA Leica MZFLIII. The images where obtained from the 40× objective and the samples were treated before the measurement with oil to enhance the performance of the equipment.

Electronic microscopy. SEM micrographs were taken on a MERLIN FE-SEM at a voltage of 1.2 kV. Samples were mounted on SEM metal stubs covered with aluminium tape by depositing drops of aqueous PMMA/VT particle dispersion and then drying in air at room temperature. TEM images were taken on a JEOL JEM-1400 at a voltage of 120 kV, using holey carbon grids were a drop of aqueous particle dispersion was deposited and dried in air at room temperature.

AFM imaging. For the AFM characterization, intermittent contact mode AFM images were obtained using an Agilent 5500 AFM/SPM microscope. The AFM probes were type NCHR silicon pointprobes (force constant ~42 N/m and resonant frequency 330 kHz) purchased from Nanoandmore GMBH. AFM image processing and rendering was performed using Gwyddion software.

Magnetization measurements. Direct current (dc) magnetic susceptibility measurements were carried out on a Quantum Design MPMS SQUID susceptometer with a 55 kG magnet and operating in the range of 1.7e320 K. All measurements were collected in a field of 10 kG. Background correction data were collected from magnetic susceptibility measurements on the holder capsules containing PMMA particles without complex 1 under exactly the same experimental conditions. Diamagnetic corrections estimated from the Pascal contents were applied to all data for determination of the molar paramagnetic susceptibilities of the compounds.

1. Dei, A. & Gatteschi, D. Molecular (nano)magnets as test grounds of quantum mechanics. *Angew. Chem. Int. Ed. Engl.* **50**, 11852–11858 (2011).
2. Evangelio, E. & Ruiz-Molina, D. Valence tautomerism: new challenges for electroactive ligands. *Eur. J. Inorg. Chem.* 2957–2971 (2005).

3. Varret, F. *et al*. Examples of molecular switching in inorganic solids, due to temperature, light, pressure, and magnetic field. *Pure. Appl. Chem.* **74**, 2159–2168 (2002).
4. Gütlich, Ph., Hauser, A. & Spiering, H. Thermal and optical switching of iron(II) complexes. *Angew. Chem. Int. Ed. Engl.* **33**, 2024–2054 (1994).
5. Sato, O., Tao, J. & Zhang, Y. –Z. Control of magnetic properties through external stimuli. *Angew. Chem. Int. Ed. Engl.* **46**, 2152–2187 (2007).
6. Kahn, O., Kröber, J. & Jay, C. Spin transition molecular materials for displays and data recording. *Adv. Mater.* **4**, 718–728 (1992).
7. Coronado *et al*. Bistable spin-crossover nanoparticles showing magnetic thermal hysteresis near room temperature. *Adv. Mat.* **19**, 1359–1361 (2007).
8. Bousseksou, A., Molnár, G., Salmon, L. & Nicolazzi, W. Molecular spin crossover phenomenon: recent achievements and prospects. *Chem. Soc. Rev.* **40**, 3313–3335 (2011).
9. Gütlich, Ph. & Dei, A. Valence tautomeric interconversion in transition metal 1,2-benzoquinone complexes. Angew. Chem. *Int. Ed. Engl.* **36**, 2734–2736 (1997).
10. Gural'skiy, I. A. *et al.* Synthesis of spin-crossover nano- and microobjects in homogeneous media. *Chem. Eur. J.* **18**, 9946–9954 (2012).
11. Imaz, I. *et al.* Valence-tautomeric metal–organic nanoparticles. *Angew. Chem. Int. Ed. Engl.* **47**, 1857–1860 (2008).
12. Forestier, T. *et al.* Nanoparticles of iron(II) spin-crossover. *Chem. Commun.* 4327–4329 (2008).
13. Galán-Mascarós *et al*. Tuning size and thermal hysteresis in bistable spin crossover nanoparticles. *Inorg. Chem.* **49**, 5706–5714 (2010).
14. Prins, F. *et al*. Room-temperature electrical addressing of a bistable spin-crossover molecular system. *Adv. Mat.* **23**, 1545–1549 (2011).
15. Létard, J. F. First evidence of the LIESST effect in a Langmuir−Blodgett film. *Inorg. Chem.* **38**, 3020–3021 (1999).
16. Seredyuk, M. *et al*. Room temperature operational thermochromic liquid crystals. *Chem Mat.* **18**, 2506–2512 (2006).
17. Cavallini, M. *et al*. Micro- and nanopatterning of spin-transition compounds into logical structures. *Angew. Chem. Int. Ed.* **47**, 8596–8600 (2008).
18. Thibault, Ch. *et al*. Soft lithographic patterning of spin crossover nanoparticles. *Langmuir* **26**, 1557–1560 (2010).
19. Molnár, G. *et al.* A combined top-down/nottom-up approach for the nanoscale patterning of spin-crossover coordination polymers. *Adv. Mat.* **19**, 2163–2167 (2007).
20. Miyamachi, T. *et al.* Robust spin crossover and memristance across a single molecule. *Nat. Commun.* **3**, 938, doi:10.1038/ncomms1940.
21. Simao, C. *et al*. A robust molecular platform for non-volatile memory devices with optical and magnetic responses. *Nature Chemistry* **3**, 359–364 (2011).
22. Forestier, Th. *et al.* Nanoparticles of [Fe(NH2-trz)3]Br2·3 H2O (NH2-trz=2-Amino-1,2,4-triazole) prepared by the reverse micelle technique: influence of particle and coherent domain sizes on spin-crossover properties. *Chem. Eur. J.* **15**, 6122–6130 (2009).
23. Rodríguez-Velamazán, J. A. *et al.* A switchable molecular rotator: neutron spectroscopy study on a polymeric spin-crossover compound. *J. Am. Chem. Soc.* **134**, 5083–5089 (2012).
24. Brooker, S. & Kitchen, J. A. Nano-magnetic materials:spin crossover compounds vs. single molecule magnets vs. single chain magnets. *Dalton Trans.* 7331–7340 (2009).
25. Hauser, A., Adler, J. & Gütlich, Ph. Light-induced excited spin state trapping (LIESST) in [Fe(2-mephen)3]2+ embedded in polymer matrices. *Chem. Phys. Lett.* **152**, 468–472 (1989).
26. Raza, Y. *et al.* Matrix-dependent cooperativity in spin crossover Fe(pyrazine)Pt(CN)4 nanoparticles Chem. *Commun.* **47**, 11501–11503 (2011).
27. Larsen, S. K. & Pierpont, C. G. Cobalt and Manganese Complexes of a Schiff Base Biquinone Radical Ligand. *J. Am. Chem. Soc.* **110**, 1827 –1832 (1988).
28. Ferlay, S., Mallah, T., Ouahes, R., Veillet, P. & Verdaguer, M. A. room-temperature organometallic magnet based on Prussian blue. *Nature* 378, 701–702 (1995).
29. Avendano *et al*. Temperature and light induced bistability in a Co3[Os(CN)6]2 6H2O Prussian Blue analog. *J. Am. Chem. Soc.* **132**, 13123–13125 (2010).
30. Evangelio, E. & Ruiz-Molina, D. Valence tautomerism: More actors than just electroactive ligands and metal ions. *C. R. Chimie* **11**, 1137–1154 (2008).
31. Kiriya, D., Chang, H.–Ch. & Kitagawa, S. Molecule-based valence tautomeric bistability synchronized with a macroscopic crystal-melt phase transition. *J. Am. Chem. Soc.* **130**, 5515–5522 (2008)
32. Mirkin, C. A. *et al.* "Dip-Pen" nanolithography. *Science* **283**, 661–663 (1999).

Acknowledgments

This work was supported by project MAT2012-38318-C03-02. F.N. thanks the MICINN for a JdC fellowship. N.V. thanks the Spanish government for her Ph.D. Fellowship support.

Author contributions

F.N. and E.E. have actively participated in both characterization experiments, supporting the rest of studies and figure editing. S.M. optimized the preparation of the thin-films. N.K. Was in charge of the NIL fabrication. P.G.-M. and E.B. were in charge of all the DPN experiments and the corresponding characterization. N.V. fabricated the PMMA particles and did the corresponding characterization. D.R.-M. supervised the project and coordinated the preparation of the manuscript. All the authors contributed to the discussion and analysis of the research in addition to actively participate in the redaction of the manuscript.

Additional information

Supplementary information accompanies this paper at http://www.nature.com/scientificreports

Competing financial interests: The authors declare no competing financial interests.

How to cite this article: Novio, F. *et al.* Robust spin crossover platforms with synchronized spin switch and polymer phase transition. *Sci. Rep.* **3**, 1708; DOI:10.1038/srep01708 (2013).